Atmos. Chem. Phys. Discuss., 11, 33419–33463, 2011
www.atmos-chem-phys-discuss.net/11/33419/2011/
doi:10.5194/acpd-11-33419-2011

Atmospheric Chemistry and Physics Discussions

Stratosphere-troposphere ozone exchange from high resolution MLS ozone analyses

J. Barré[1], V.-H. Peuch[1], J.-L. Attié[1,2], L. El Amraoui[1], W. A. Lahoz[1,3], B. Josse[1], M. Claeyman[1,2], and P. Nédélec[2]

[1]CNRM-GAME, Météo-France and CNRS URA1357, Toulouse, France
[2]Laboratoire d'Aérologie, Université de Toulouse, CNRS/INSU, Toulouse, France
[3]NILU, 2027 Kjeller, Norway

Received: 8 November 2011 – Accepted: 12 December 2011 – Published: 19 December 2011

Correspondence to: J. Barré (jerome.barre@meteo.fr)

Published by Copernicus Publications on behalf of the European Geosciences Union.

Abstract

We assimilate stratospheric ozone profiles from MLS (Microwave Limb Sounder) into the MOCAGE CTM model in order to study Stratosphere-Troposphere Exchange (STE). This study uses two horizontal grid resolution of 2° and 0.2°. The combined impacts of MLS ozone assimilation and high horizontal resolution are illustrated in two case studies where STE events occurred (23 June 2009 and 17 July 2009). At high resolution the fine filamentary structures of stratospheric air which characterise STE events are captured by the model. To test the impact of the assimilation and the resolution, we compare model outputs from different experiments (high resolution and low resolution; MLS assimilation run and free run) with independent data (MOZAIC aircraft ozone data; WOUDC ozone sonde network data) not used in the assimilation. MLS ozone analyses show a better description of the UTLS region and the stratospheric intrusions than the free model run. In particular, at high horizontal resolution the high resolution MLS ozone analyses presents fine filamentary ozone structures at the UTLS and laminae structures in the tropospheric ozone profile. By using MLS ozone analyses and high resolution, ozone fluxes through the tropopause show a range of results that lie within the range of similar previous studies. Results from backward trajectories and forecasts results show that assimilation at high horizontal resolution of MLS ozone profiles between 10 hPa and 215 hPa has an impact on tropospheric ozone.

1 Introduction

In the stratosphere, ozone (O_3) is known to shield the surface from harmful ultraviolet radiation. In the middle and high troposphere ozone is the third most important greenhouse gas after carbon dioxide (CO_2) and methane (CH_4). Its forcing is equivalent to about 24 % of that from carbon dioxide (Ramaswamy et al., 2001). The troposphere and stratosphere are characterised by different dynamical and chemical properties, with strong gradients of potential vorticity (PV) and ozone at the tropopause.

ACPD
11, 33419–33463, 2011

Stratosphere-troposphere exchange (STE) events play a key role in controlling the ozone budget in the Upper Troposphere/Lower Stratosphere (UTLS) (Holton et al., 1995), which in turn affects the radiation budget (IPCC 1996). The stratosphere is characterised by significantly high values of PV and ozone concentrations, so intrusion of stratospheric air is expected to bring PV and ozone rich air into the troposphere. These intrusions typically form filamentary structures, which appear as laminae in the ozone profiles and often exhibit mesoscale features (Holton et al., 1995; Stohl et al., 2003). Fine scale filamentary structures of PV and ozone at lower stratosphere have been simulated by Hauchecorne et al. (2002), Marchand et al. (2003) and Tripathi et al. (2006) and show that high resolution simulations are needed for detailed investigation.

In the UTLS region and on the timescale of a few days, PV and ozone are quasi-conserved parameters (Appenzeller et al., 1996). In addition, Beekmann et al. (1994) have shown that ozone fields and PV fields are strongly correlated in the UTLS layers of the atmosphere. These properties have been used to estimate cross-tropopause ozone fluxes for STE events. These estimates are typically performed using regional scale models, and exhibit a broad range of values (Büker et al., 2005; Ebel et al., 1991). This variability in the flux estimates is due to the type of model (Eulerian or Lagrangian); the method of calculation; and other parameters such as domain size, timescale and heterogeneity of synoptic scale events that transport different amounts of ozone. In the last few decades different methods have been used to investigate the flux of chemical species (in particular ozone) across the tropopause. For example, Olsen et al. (2002) and Olsen et al. (2003) have made an estimation of the global ozone flux by a correlation method between PV and O_3 values. Jing et al. (2004) estimate the flux by using the contour advection technique which requires a Lagrangian advection scheme. In this study, we use the method established by Wei (1987) for diagnosing the flux through the tropopause in an Eulerian approach. This method was also used by Grewe and Dameris (1996), Clark et al. (2007) and more recently at high resolution by Luk'yanov et al. (2009).

ACPD
11, 33419–33463, 2011

Ozone fields in the UTLS region have strong vertical gradients. The representation of these gradients is a well-known limitation of most of the chemical transport models (CTM) as described by Law et al. (2000). Ozone measurements from the Microwave Limb Sounder (MLS) instrument onboard the Aura satellite give global coverage, and are able to detect stratospheric profiles between 215 and 0.46 hPa. Comparisons of simulated ozone fields with MLS ozone observations show good agreement in the UTLS spatial structure (Leblanc et al., 2006) and suggest that stratospheric intrusions can be captured by MLS. Due to the sparse horizontal sampling of these profiles, MLS ozone products are not able to resolve the synoptic-scale variabilities in the tropopause region. To solve this issue we use data assimilation which combines observational information with a priori information from a model in an objective way (Kalnay, 2003). Data assimilation of stratospheric ozone profiles from satellite data has been used extensively to study the UTLS distribution of ozone (Semane et al., 2007; El Amraoui et al., 2010; Wargan et al., 2010). These studies show that ozone analyses from assimilation of limb sounder ozone data can capture the signature of stratospheric intrusions in a realistic way.

In this paper we use the MOCAGE-PALM system of Météo-France to assimilate MLS ozone data into the MOCAGE (MOdèle de Chimie Atmospherique à Grande Echelle) CTM (Peuch et al., 1999). The aim is to have a better representation of the STE by increasing the horizontal grid model resolution from 2° to 0.2°. In addition, we improve the representation of the STE by assimilating MLS ozone data. In order to investigate STE in detail, two typical cases studies are presented and validated with independent aircraft and balloon data. For these two case studies, we estimate the ozone flux across the tropopause. Finally, we show that estimates of STE are significantly modified by the model resolution and the MLS ozone assimilation. The outline of the paper is as follows: Section 2 describes the MOCAGE CTM and the assimilation method. Section 3 presents the impact of MLS ozone assimilation in the MOCAGE model. In Sect. 4, results of two case studies of STE are presented. The validation with independent data and the ozone flux estimation at the tropopause are discussed. Before concluding,

ACPD
11, 33419–33463, 2011

we discuss in Sect. 5 the impact of high resolution and MLS ozone assimilation on tropospheric ozone.

2 Methodology

2.1 CTM model

The MOCAGE model is a three-dimensional CTM for the troposphere and the stratosphere (Peuch et al., 1999) which simulates the interactions between the physical and chemical processes. It uses a semi-Lagrangian advection scheme (Josse et al., 2004) to transport the chemical species. It has 47 hybrid levels from the surface to ~5 hPa with a resolution of about 150 m in the lower troposphere increasing to 800 m in the higher troposphere. Turbulent diffusion is calculated with the scheme of Louis (1979) and convective processes with the scheme of Bechtold et al. (2001). The chemical scheme used in this study is RACMOBUS. It is a combination of the stratospheric scheme REPROBUS (Lefèvre et al., 1994) and the tropospheric scheme RACM (Stockwell et al., 1997). It includes 119 individual species with 89 prognostic variables and 372 chemical reactions. MOCAGE has the flexibility to be used for stratospheric studies (El Amraoui et al., 2008a) and tropospheric studies (Dufour et al., 2005). It is used in the operational air quality monitoring system in France: Prev'air (Rouïl et al., 2008) and in the pre-operational GMES (Global Monitoring for Environment and Security) atmospheric core service (Hollingsworth et al., 2008). A detailed validation of the model has been done using a large number of measurements during the Intercontinental Transport of Ozone and Precursors (ICARTT/ITOP) campaign (Bousserez et al., 2007). The meteorological analyses of Météo-France, ARPEGE (Courtier et al., 1991) are used to force the dynamics of the model every 3 h. To force the model, ARPEGE analyses are interpolated on the MOCAGE grid. The resolution of ARPEGE analyses are in a T798 spectral grid (i.e. resolution from 10.5 km over France to 60 km over the South Pacific). Moreover, MOCAGE has the possibility to be in tracer mode and to specify the

ACPD
11, 33419–33463, 2011

temporal and geometrical characteristics of a tracer release. An interesting additional capability of MOCAGE is to calculate backwards 3-D simulations, using its adjoint.

In this study, the model uses 2 domains: a global domain at 2° (low horizontal resolution: LR) and a regional nested domain at 0.2° (high horizontal resolution: HR) over Europe, from 32° N to 72° N and from 16° W to 36° E. Four modelling experiments are performed:

1. low resolution free model run,
2. low resolution MLS ozone analysis,
3. high resolution free model run,
4. high resolution MLS ozone analysis.

The simulations in this paper cover the period from 1 June 2009 to 1 September 2009. The assimilation experiment started on 1 June 2009. The initialisation field for this date has been obtained from a free model run started from the April climatological initial field. We thus have a free model run spin-up of 2 months in addition to 1 month of MLS data assimilation before the 1 June 2009.

2.2 Data assimilation system

The assimilation system used in this study is MOCAGE-PALM implemented within the PALM framework (Buis et al., 2006). The technique used is 3D-FGAT (First Guess at Appropriate Time, Fisher and Andersson, 2001). This technique is a compromise between the 3D-Var (3-D-variational) and the 4D-Var (4-D-variational) methods. It compares the observation and background at the correct time and assumes that the increment to be added to the background state is constant over the entire assimilation window. The choice of this technique limits the size of the assimilation window, since it has to be short enough compared to chemistry and transport timescales. It has been validated during the assimilation of ENVISAT data project (ASSET, Lahoz et al., 2007)

ACPD
11, 33419–33463, 2011

and has produced good quality results compared to independent data and other assimilation systems (Geer et al., 2006). MOCAGE-PALM have been used to assess the quality of satellite ozone measurements (Massart et al., 2007). It has also been proven to be useful to overcome the possible deficiencies of the model. In this context, assimilation products has been used in many atmospheric studies in relation to the ozone loss in the Arctic vortex (El Amraoui et al., 2008a), the tropics-mid-latitudes exchanges (Bencherif et al., 2007), the STE (Semane et al., 2007), the exchange between the polar vortex and the mid-latitudes (El Amraoui et al., 2008b), and diagnosing STE from ozone and carbon monoxide fields (El Amraoui et al., 2010).

2.3 Aura/MLS ozone observations

The Aura satellite was launched on 15 July 2004 and placed into a near-polar Earth orbit at ~705 km with an inclination of 98° and an ascending node at 13:45 UT. It makes about 14 orbits per day. The MLS instrument onboard Aura uses the microwave limb sounding technique to measure chemical constituents and dynamical tracers between the upper troposphere and the lower mesosphere (Waters et al., 2006). It provides dense spatial coverage with 3500 profiles daily between 82° N and 82° S. In this study we use the Version 2.2 of the MLS O_3 dataset. It is a standard retrieval between 215 and 0.46 hPa with a vertical resolution of 3 km in the upper troposphere and the stratosphere. For ozone measurements the along-track resolution is ~200 km and the cross-track resolution is ~6 km between 215 and 10 hPa. The estimated single profile precision in the extra-tropical UTLS region is of the order of 0.04 ppmv (parts per million by volume) from 215 to 100 hPa and between 0.05 and 0.2 ppmv from 46 to 10 hPa (Froidevaux et al., 2008). For the assimilation experiment, MLS data are selected according to the precision and quality flags recommended in the MLS Version 2.2 Level data quality and description document (see http://mls.jpl.nasa.gov/data/v2-2_data_quality_document.pdf). The respective errors for each profile are taken into account in the assimilation process through the error covariance matrix of observations. Note that only measurements performed between

ACPD
11, 33419–33463, 2011

215 and 10 hPa are used during the assimilation experiment because of the limitation imposed by the upper boundary (5 hPa) of the MOCAGE version used in this paper.

3 MLS assimilation

In this section, we show the impact on the MOCAGE model of MLS ozone data assimilation. Assimilation increments, (i.e. the difference between the first guess fields and the analysis, in the assimilation window time step) increase the ozone concentrations at middle and polar latitudes in the lower stratosphere. Figure 1 (left hand panel) shows mean increments of MLS ozone assimilation for July 2009, zonally averaged over Europe in a relative difference in as a percentage of the ratio increments/free run for the HR runs. MLS ozone profiles are between 10 and 215 hPa, thus the increment is only located at these levels. The strongest increments are located between 200 and 300 hPa and 45° N and 72° N. This figure (right hand panel) also shows relative difference in % between the free run field and the MLS ozone analysis field, zonally averaged over Europe for July 2009 (i.e. free run-MLS analysis/free run). Compared to the assimilation increments, major differences between the free run and the analyses fields occur in the same region: between 200 and 300 hPa and 45° N and 70° N, however the impact of this difference in the troposphere is significant. Positive differences with values around 20 % between 1000 hPa and 300 hPa and 40° N and 72° N do not occur in assimilation increments. These differences observed in troposphere are the result of the southward cross-tropopause advection of lower stratospheric air masses with increased ozone values.

Impacts of MLS assimilation in the troposphere can be extended and generalised at global scale. Figure 2 presents zonal means of ozone over the Northern Hemisphere for July 2009, for free model run (left hand side panel) and MLS ozone analysis (right hand side panel) for LR runs. Black lines delineate the potential temperature iso-lines, the white lines delineate the 2 PVU iso-lines (1 PVU = 1×10^6 K kg^{-1} m^2 s^{-1}). For the mid and polar latitudes, stratospheric rich ozone air is located above 350 K.

ACPD
11, 33419–33463, 2011

In the stratosphere MLS ozone analysis values are higher than the free run values for the levels located between 330 K and 370 K. Isentropic lines (i.e. potential temperature lines) between 320 K and 340 K cross the 2 PVU iso-lines (i.e. a tropopause height estimation), and go downward between 300 hPa and 600 hPa at mid-latitudes. These lines give an idea of the mean isentropic processes during July 2009. STEs are considered as an irreversible isentropes process in the lowermost stratosphere, where the isentropics cross the tropopause (Postel and Hitchman, 1999). Subsequent southward cross-tropopause advection of these increments during a STE event increases ozone concentrations in the analyses at the location of the intrusion. This will be reflected in the case studies presented below, which show that the analyses have higher ozone values than the free model run at the location of the intrusion, whereas the PV patterns are unchanged. Within the framework of assimilation in a CTM model, the ozone distribution in the stratosphere and the troposphere is modified by the MLS ozone analyses, whereas dynamical information shown here by the 2 PVU iso-line is not.

4 Results

4.1 Filament processes

In this section we focus on 2 STE case studies called streamers. Streamers which can be identified as filamentary structures of stratospheric air in the UTLS, have been characterised by Appenzeller and Davies (1992), and Appenzeller et al. (1996) with the help of water vapour satellite measurements. These patterns with high PV values (but also with high ozone values and low specific humidity), with a sub-synoptic scale or a mesoscale, can stretch southward in an irreversible way, with a length of 2000 km to 3000 km and a maximum width of 200 km. These streamers are generated by the Rossby wave breaking at mid latitudes (Postel and Hitchman, 1999). Streamers are considered as an irreversible isentropic process (see Sect. 3), and as a middle scale mass exchange mechanism between the stratosphere and the troposphere.

ACPD
11, 33419–33463, 2011

Two types of streamers are defined (Thorncroft et al., 1993): Type I has an anticyclonic curve (linked to an anticyclone at its western edge) and can often break into a train of eddies which also means a PV height anomaly train (Browning, 1993). These eddies rolling up the stratospheric air with the tropospheric air, which allows a favourable mixing situation by increasing the surface between the two air masses. Type II has a North-South orientation following a cold front stretching at the surface, with a vortex at the southern tip (Appenzeller et al., 1996). A stretching equatorward thalweg often means downstream deep convection, which can generate mass transfers between stratosphere and troposphere.

4.2 Meteorological situation

4.2.1 Case 1: stratospheric intrusion on 23 June 2009

In this section, we describe a stratospheric intrusion which took place on 23 June 2009 over Europe and lasted 4.5 days (from 20 June, 06:00 UT, to 24 June, 18:00 UT). Figure 3a shows horizontal distribution (left hand side panels) and vertical cross-sections (right hand side panels) of PV during the main phase of the intrusion (23 June 2009, 12:00 UT) at two model resolutions (LR: 2°, HR: 0.2°). Characteristic signatures of the intruded air are high PV. This pattern can be associated as a type I streamer described above (see Sect. 4.1). It has an anticyclonic curve (Fig. 3b) and a NE-SW orientation from the North of the Baltic sea to the centre of France. A train of eddies is nearly visible at the South tip of the streamer. On 23 June 2009 12:00 UT and with a resolution of 0.2° these eddies are not clearly visible. PV fields (HR and LR), show high PV values intruding the troposphere. As expected, at upper tropospheric levels (200 hPa–300 hPa) PV values increase between the longitude range 5° E–25° E due to the strong cyclonic (Fig. 3b) PV anomaly occurring above. The vertical distribution shows high stratospheric PV values (>2 PVU) below 300 hPa. At these pressure levels, rapid mixing by turbulence and convection may lead to irreversible STE events (Gouget et al., 2000).

ACPD
11, 33419–33463, 2011

4.2.2 Case 2: stratospheric intrusion on 17 July 2009

This case describes a stratospheric intrusion which took place on 17 July 2009 over Europe and lasted 3.5 days (from 16 July, 06:00 UT, to 19 July, 18:00 UT). Figure 4b shows the horizontal distribution (left hand side panels) and the longitude-pressure cross-sections (right hand side panels) of PV during the main phase of the intrusion (17 July 2009, 15:00 UT) at the two model horizontal resolutions. This pattern can be associated as a type II streamer described above (see Sect. 4.1). The streamer has a more North-South orientation than the previous case study (see Sect. 4.2.2), from the North of Ireland to the South of France. A South tip vortex over France is visible at HR. Vertical structure shows a deep intrusion. PV fields (HR and LR), show a V-shaped intrusion, due to the cross section orientation. As expected, at upper tropospheric levels (200 hPa–300 hPa) PV values increases between the longitude range 15° W–8° E due to the strong cyclonic (Fig. 4a) PV anomaly occurring above. The vertical distribution shows high stratospheric PV values (>2 PVU) below 400 hPa.

4.2.3 Comparison between the low resolution and the high resolution runs

In this section we compare the PV fields from the LR runs and HR runs. On horizontal distributions, the HR allows an accurate representation of the streamers in the horizontal distributions. Horizontal gradients are increased with the HR whereas the LR gives a very smooth representation of these streamers. For example in the case of 23 June 2009 the LR horizontal PV field show high values (PV anomaly) over Italy and South-East of France which do not seem to be linked by a streamer to the polar stratospheric air mass. The HR horizontal distributions of PV allow the representation in the UTLS of the filamentary structures that characterise the streamers. Fine vertical structures in the streamers are also captured in the HR runs. In both cases we notice a vertical PV filamentary structure occurring at HR to the west of the PV height anomaly described in Sects. 4.2.1 and 4.2.2 (5° E in case 1 and 5° W in case 2). At LR, these vertical structures are somewhat seen in case 2 but not captured in case 1.

ACPD
11, 33419–33463, 2011

4.3 Ozone analysis fields

Figures 5 and 6 show horizontal distributions (left hand side panels) and vertical cross-sections (right hand side panels) of ozone during the main phase of the intrusions for case 1 (23 June 2009, 12:00 UT) and case 2 (17 July 2009, 15:00 UT) respectively. Figures 5 and 6 compares the free model experiment and the analyses from the assimilation experiment, at two model resolutions (see Sect. 2.1). White solid lines identify the 2 PVU iso-line, which is often used to define the dynamical tropopause. Ozone fields and PV fields show similar patterns. These patterns are seen in the free run experiments but more marked in the MLS assimilation runs. In horizontal distributions, MLS ozone analyses show higher ozone values than the free runs. Generally the vertical cross sections from MLS ozone analyses show the vertical ozone gradient pulled down in altitude where the STE takes place. The shape of the vertical ozone gradient in MLS ozone analyses follows more closely the 2 PVU iso-line. MLS ozone analyses bring to the model an added value to the ozone distribution at the UTLS layers. Analysed ozone fields show more agreement with PV fields than free run ozone fields.

Regarding the improvement shown by the HR fields, we can conclude as for Sect. 4.2.3. Filamentary structures which cannot be seen or are smoothed in the LR runs are represented accurately in the HR runs. For example, in case 1, the NE-SW ozone filament over northern Europe is visible in the HR horizontal distribution only. This filament is seen in the vertical cross-sections as the vertical ozone tropospheric patterns at 5° E between 300 and 500 hPa for the HR MLS ozone analysis. In case 2, the NE-SW ozone filament over the Mediterranean sea is only seen on the HR horizontal distribution. This filament corresponds in the longitude-pressure cross sections to the vertical high volume mixing ratio (VMR) of ozone tropospheric patterns visible at 13° E and between 300 and 500 hPa for the HR MLS ozone analysis.

ACPD
11, 33419–33463, 2011

To summarise, these filamentary structures of ozone visible at the HR runs are smoothed or not well represented in the LR runs. At HR, ozone filamentary patterns are more marked in the MLS ozone analyses. These filamentary structures come from the lower stratosphere at polar and middle latitudes where the MLS increments (relative values in %) are the largest (see Sect. 3).

4.4 Comparison with independent datasets

In this section a validation of MLS ozone analyses during two case studies is performed using the WOUDC (World Ozone and Ultraviolet Radiation Data Centre) ozone sondes and the MOZAIC (Measurements of OZone, water vapour, carbon monoxide and nitrogen oxides by in-service AIrbus airCraft) aircraft flights. The MOZAIC program measures ozone and other species from commercial aircraft (Marenco et al., 1998). Comparison of the first two years of MOZAIC ozone data with ozone sonde network data showed good agreement (Thouret et al., 1998). The WOUDC is one of the five World Data Centres which are part of the Global Atmosphere Watch (GAW) program of the World Meteorological Organization (WMO).

4.4.1 Case 1: stratospheric intrusion on 23 June 2009

In this case study two MOZAIC flights have been used: a flight on 23 June 2009 from Frankfurt (50° N, 8° E, Germany) at 08:13 UT to Calgary (51° N, 114° W, Canada) and a flight on 23 June 2009 from Frankfurt (50° N, 8° E, Germany) at 13:00 UT to Philadelphia (39° N, 75° W, US). In Fig. 7 (left hand side panel), the runs at HR (solid lines) agree better with MOZAIC data (green line) than the LR runs (dashed lines). The two MOZAIC flights track cross the filament near 5° W and 52° N and detect a peak of ozone at this location. The use of HR improves considerably the ozone distribution. Peaks detected by the MOZAIC flights are well represented by the HR runs. Where the analyses and free model run fields at HR show the signature of the filament, the analyses are significantly closer to the MOZAIC data. This comparison shows that the MLS ozone analysed fields at HR improve the representation of UTLS ozone during a stratospheric intrusion event.

ACPD
11, 33419–33463, 2011

Unfortunately there are no WOUDC vertical records well co-located in space and time with the stratospheric intrusion event. We thus compare our results with a sonde launched at Legionowo (Poland: 52.4° N, 21° E) at 11:17 UT on 24 June 2009. In Fig. 8, the ozone sonde measurements (green line) are compared with the four different experiments in this study. These profiles show that between 100 hPa and 300 hPa MLS ozone analyses are in better agreement with observations than the free run. In this height range, the improvement of the HR MLS ozone analyses is characterised by a maximum closer to the observations than for the LR MLS ozone analyses. Compared to the tropospheric values, MLS ozone analyses show no improvement but increase the positive bias already seen in the free model runs.

4.4.2 Case 2: stratospheric intrusion on 17 July 2009

The MOZAIC ozone data used in this study comes from a flight on 17 July 2009 from Frankfurt (50° N, 8° E, Germany at 11:57 UT to Atlanta (33° N, 84° W, US) and left the regional domain at 14:16 UT. In Fig. 9 (left hand side panel), the ozone analyses (red lines) agree better with MOZAIC data (green line) than the free model (blue lines). The MOZAIC flight track crosses the intrusion between 3.5° E and 1.5° W. At the location where the analyses and free model fields show the signature of the intrusion, the analyses are significantly closer to the MOZAIC data. This comparison shows that the MLS ozone analysed fields generally improves the UTLS ozone representation in the stratospheric intrusion. High resolution results (solid lines) do not show significant improvement in this figure, but seems to be consistent with low resolution results (dashed lines).

At 11:00 UT on 17 July 2009, a MeteoSwiss ozone sonde was launched from Payerne (Switzerland; 46.5° N, 6.6° E). In Fig. 10, the ozone sonde measurements (green line) are compared with the four different experiments in this study. Figure 10 shows a maximum located at 190 hPa in the UTLS. The analyses at high resolution are closer to the ozone sonde data in terms of magnitude and variability with height providing the best match with the ozone profile changes on the vertical. This maximum represents

ACPD
11, 33419–33463, 2011

the east side of the V-shaped intrusion identified on the left hand side panel of Fig. 6. HR analyses improve the representation of this maximum. A second maximum located at 500 hPa is only represented by the MLS ozone analyses at HR. The ozone sonde measurement is co-located with a tropospheric filament of ozone. Holton et al. (1995) and Stohl et al. (2003) have shown that stratospheric intrusions typically form filamentary structures in the free troposphere, which appear as laminae in the ozone profile. This tropospheric maximum comes from a stratospheric intrusion that occurred few days before in Northern latitudes. A discussion of the origin of this maximum of ozone is detailed below. This tropospheric ozone maximum shows the benefits of HR MLS ozone analyses in the troposphere. Validation with independent datasets shows that fine horizontal structures at the UTLS are well captured by HR MLS ozone analyses (Fig. 7). Vertical structure is improved in the UTLS and in the free troposphere appearing as laminae in the ozone profile (Figs. 8 and 10). Results indicate that the improvement in the representation of the UTLS and free troposphere structures is owing to the use of assimilation and HR.

4.4.3 Impact in the troposphere

Between about 300 hPa and 800 hPa, in the free troposphere, the free model run at HR is closer than HR MLS ozone analyses to the ozone sonde data in terms of magnitude. In other words the MLS ozone analyses increase the positive bias in the troposphere which already exists in the free runs. This suggest that too much stratospheric ozone is advected through the tropopause. The high horizontal resolution used in this study is still too coarse to represent faithfully the filamentary structures of ozone in the UTLS measured by MOZAIC aircraft. For example in case study 2 (Fig. 7), the observed filament is very thin and horizontal ozone gradients around are very strong. MLS ozone analyses with 0.2° (~20 km) horizontal resolution have hourly temporal resolution while the MOZAIC data has a sampling frequency of 4 s corresponding to a distance of 1 km between each measurements. The MLS ozone analyses are able to have a good estimation of the maximum values, but spatial gradients are smoothed. Then MLS

ACPD
11, 33419–33463, 2011

ozone analyses have a positive bias in the neighbourhood of the filaments. This means fine structures in the ozone analyses contain too much ozone in the UTLS layers. This suggest that MLS ozone analyses bring more ozone from stratosphere to troposphere than the free run. This overestimation of ozone values is stronger at LR than at HR, due to the resolution. This also suggest that LR brings more ozone from stratosphere to troposphere than HR.

The MLS ozone analyses are closer to the MOZAIC ozone data than the free model run in the UTLS layers. Moreover HR adds fine horizontal and vertical structures which are amplified by the MLS ozone analyses. Ozone fluxes in the UTLS region should be modified by the assimilation and by the increase in horizontal resolution. These fluxes are estimated in the next section.

4.5 Stratosphere-troposphere ozone fluxes

4.5.1 Methodology

In this section, we focus on the calculation of the net ozone flux across the tropopause in order to quantify the importance of the STE events according to the horizontal resolution used. There are many ways to estimate the flux of ozone across the tropopause, for example, by correlation of concentrations of nitrous oxide (N_2O) with O_3 (Murphy and Fahey, 1994) or by correlation of ozone column and PV column (Olsen et al., 2002, 2003), the contour advection technique (Jing et al., 2004), or chemical transport modelling (Crutzen et al., 1999). In this study, we apply the formulae of Wei (1987) and as described by Grewe and Dameris (1996) to calculate the net ozone flux using MOCAGE CTM for the various runs. This method has already been applied by Clark et al. (2007) using MOZAIC data assimilated into MOCAGE at global scale and at HR. The method simply requires dynamical information and ozone concentration from the model.

ACPD
11, 33419–33463, 2011

The formulae can be expressed with pressure as vertical coordinate as follows:

$$F_p(O_3) = -g^{-1} \cdot [O_3] \left(\omega - \frac{\partial p_{\text{trop}}}{\partial t} - V_h \cdot \nabla_{\text{trop}} \cdot p_{\text{trop}} \right) \quad (1)$$

with g the acceleration of gravity, $[O_3]$ the ozone mixing ratio at the tropopause layer, $\omega = dp/dt$ the vertical wind in pressure coordinates, p_{trop} the tropopause height in pressure coordinates, and V_h the horizontal wind. The required dynamical and chemical information is provided by the ARPEGE and MOCAGE models, respectively.

For the calculation of the STE net flux using Eq. (1) we need to determine the height of the dynamical tropopause. We performed a sensitivity study of the height of the dynamical tropopause using different PV values. The mid-latitude tropopause is generally found between 1.6 PVU (World Meteorological Organization, 1986) and 3.5 PVU (Hoerling et al., 1991) and to be in this range, we use a value between 1.5 PVU and 2.5 PVU. Multiple tropopauses criteria can exist at a given location. In this study, we define the tropopause at the highest height where the tropopause criteria are met. Such a condition truncates the tropopause fold at its onset; therefore, any stratospheric air entering a fold is assumed to be irreversibly transferred to the troposphere. After determining the height of the tropopause in time and space, the STE net ozone flux across this surface is calculated.

STE net ozone flux calculation is performed with the 4 modelling experiments. The modelling time step is 3 h and the calculation is performed for each case period (see Sect. 4.2) on a square area between 32° N–60° N and 0° W–27° E (1×10^6 km^2) for case 1 and for case 2 on a square area between 35° N–65° N and 16° W–29° E (1.6×10^6 km^2). Because this study focuses on singulars STE events, the choice of the area is defined by the location of the streamer.

4.5.2 Ozone flux results

In order to assess the importance of the PV value on the flux calculation, we made the calculation on a varying PV tropopause surface between 1.5 and 2.5 PVU. Figure 11

ACPD
11, 33419–33463, 2011

presents flux calculations averaged in space (square area defined in Sect. 4.5.1) and time (see Sect. 4.2) for the two case studies, averaged over space (square area defined in Sect. 4.5.1) and time (duration defined in Sects. 4.2.1 and 4.2.2). For each modelling experiment, results show the same order of magnitude for a varying PV surface. The flux is modified through the assimilation of the MLS ozone observations and the different horizontal resolutions. Low resolution results show net ozone flux with values between 0.5×10^{-10} kg m^{-2} s^{-1} and 2.0×10^{-10} kg m^{-2} s^{-1} whereas HR results shows flux values between 0.2×10^{-10} kg m^{-2} s^{-1} and 0.5×10^{-10} kg m^{-2} s^{-1}. We calculated the averaged relative difference between the ozone flux from the runs (free run and MLS ozone analyses) with the two resolutions (Table 1). The high resolution tends to decrease the ozone flux values whereas MLS ozone assimilation tends to increase the flux values. Compared to the LR free run, LR ozone assimilation increases the fluxes by 86 % for case 1 and by 109 % in case 2. Compared to the HR free run, HR ozone assimilation increases the fluxes by 30 % for case 1 and by 56 % in case 2. The impact of MLS ozone assimilation is different between the two cases studies. MLS assimilation has more impact on case 2 than in case 1. This is explained by a stronger enhancement of the ozone STE pattern in MLS ozone analyses in case study 2 (see Figs. 5 and 6). Ozone values are more increased in case 1 than in case 2. Then more ozone is advected in troposphere in case 2. MLS ozone analyses have a different contribution in time and space, this has an impact on flux calculations. In Sect. 4.4.3 we have shown that MOCAGE has difficulties to represent very strong gradients when the resolution is too coarse. This smoothed gradient representation overestimates ozone fields in UTLS when analyses has its maximum values increased to reach the values seen in the independent datasets. We also shown in Sect. 4.4.3 that effect is more marked at LR than at HR. UTLS ozone overestimation is larger at LR MLS ozone analyses than at HR ozone analyses. With the increase of ozone values at a coarser resolution we can easily understand that in both case studies, the MLS ozone analyses increase more the fluxes at LR than at HR. Compared to the LR free run, the HR free run decreases the fluxes by similar values for case 1 and for case 2, 63 % and 68 % respectively.

ACPD
11, 33419–33463, 2011

Compared to the LR analyses, the HR analyses decreases the fluxes by 74 % for case 1 and 76 % for case 2. We can notice how close are the values between case 1 and case 2. In any case, increasing the resolution decreases the STE ozone net flux in a consistent way.

Over the past 20 yr, several studies, using varying domains, time periods and horizontal resolution, have estimated STE fluxes. For example, Büker et al. (2005), Hitchman et al. (2003) and Lamarque and Hess (1994) worked on similar events, over similar latitudes and using models with a horizontal resolution of the order of 1° and they estimated STE fluxes of $2.05 \times {}^{-10}\,\mathrm{kg\,m^{-2}\,s^{-1}}$ (domain size: $9 \times 10^6\,\mathrm{km^2}$, duration: 2.5 days), $3.24 \times {}^{-10}\,\mathrm{kg\,m^{-2}\,s^{-1}}$ (domain size: $2.5 \times 10^7\,\mathrm{km^2}$, duration: 1 day), $1.06 \times {}^{-10}\,\mathrm{kg\,m^{-2}\,s^{-1}}$ (domain size: $3 \times 10^6\,\mathrm{km^2}$, duration: 3 days), respectively. Luk'yanov et al. (2009) used the Wei method (Wei, 1987) on a horizontal grid resolution of 0.25° and estimated an STE ozone flux of $0.94 \times 10^{-10}\,\mathrm{kg\,m^{-2}\,s^{-1}}$ (domain size: $1.6 \times 10^6\,\mathrm{km^2}$, duration: 1 day). These latter values are of the same order of magnitude as values found by Ancellet et al. (1991) using LIDAR measurements ($0.61 \times 10^{-10}\,\mathrm{kg\,m^{-2}\,s^{-1}}$, duration: 2.5 days). These previous studies and the present study differ in many ways: domain size, location, duration, calculation method, model resolution, period of the year, etc. These parameters have an influence in the flux estimates and comparisons between these studies have to be taken with caution. Low resolution results give STE net ozone flux values between $0.5 \times 10^{-10}\,\mathrm{kg\,m^{-2}\,s^{-1}}$ and $2.0 \times 10^{-10}\,\mathrm{kg\,m^{-2}\,s^{-1}}$. These values lie in the range of the previous studies with a horizontal resolution similar to 2° (Büker et al., 2005; Hitchman et al., 2003; Lamarque and Hess, 1994). High resolution results give STE flux values between $0.2 \times 10^{-10}\,\mathrm{kg\,m^{-2}\,s^{-1}}$ and $0.5 \times 10^{-10}\,\mathrm{kg\,m^{-2}\,s^{-1}}$. The values given by the HR runs are closer to Luk'yanov et al. (2009) results, which use an horizontal resolution of 0.25°, and Ancellet et al. (1991) estimates from LIDAR measurements.

As mentioned in Sect. 4.4.3, MLS analyses overestimate the ozone concentrations when independent data show strong gradients in the vertical and in the horizontal. This overestimation of ozone is more important at LR than at HR and responsible for

ACPD
11, 33419–33463, 2011

an increasing tropospheric positive bias. As expected the fluxes are increased with MLS assimilation and thus overestimated. Within the context of the published literature on STE ozone fluxes, the fluxes estimated from MLS ozone analyses have a realistic order of magnitude.

5 Tropospheric impact of MLS ozone analyses at high resolution

5.1 Backward trajectories: impact of high resolution

In this section we use MOCAGE to calculate backward trajectories in the situation of the case study 2 (17 July 2009). The tracer was initialised between 400 and 600 hPa on 17 July 2009 at 11:00 UT where a tropospheric laminae structure was observed by the WOUDC profile and was reasonably well represented by the HR MLS ozone analyses (see Sect. 4.4.2 and Fig. 10). Moreover, the model is initialised for the global domain (LR) and for the regional domain (HR). Note that the global domain is used to constrain the regional domain. Figure 12 shows the zonal means of tracer concentration in the Northern Hemisphere. We observe difference in the backward trajectories for the two experiments on 12 July 2009 at 00:00 UT, five and a half days earlier, the sounding at Payerne was made. We observe a larger part of the tracers around the polar UTLS for the HR run whereas it is less evident for the LR run where the larger part of the tracers are instead located in the mid troposphere at middle latitudes. The LR run presents a part of the tracers close to the surface around 42° N. Different to the LR run, the HR run clearly shows that the lamina structure at 500 hPa mentioned above, originates from the polar UTLS.

5.2 Ozone forecasts at high resolution: impact of MLS ozone analyses

In order to quantify the tropospheric impact of the MLS assimilation on the stratosphere, a forecast of two weeks has been done. The initial state is the MLS ozone analyses on

ACPD
11, 33419–33463, 2011

15 July 2009 00:00 UT and the forecast ends 14 days later on 29 July 2009 00:00 UT. At first we compare the forecast to the WOUDC profile at Payerne on 17 July 2009 11:00 UT (Fig. 13). Two and a half days after the beginning of the forecast, the maximum of ozone in the UTLS decreases but the stratospheric and the free tropospheric profiles show no significant changes. As already shown in Fig. 1 the largest impact of MLS is located in the UTLS region. The transport of ozone from UTLS to the free troposphere takes a few days. The advantage of MLS ozone analyses (e.g. revealing ozone features in the free troposphere) can be used to forecast the free troposphere for about a week. Figure 14 shows the relative difference between forecasts and the MLS ozone analyses until the end of July. The largest difference is located at the UTLS layers and increases with time. In the first seven days of the forecast the difference in the free troposphere (below 300 hPa) is very small, under 5 %. By constraining ozone at the UTLS, tropospheric forecasts still contain after 7 days a strong contribution from the MLS observations. By using MLS ozone analyses at high resolution these tropospheric features (e.g. laminae of ozone structures in tropospheric profiles) can be forecast for a week. Even if MLS ozone analyses are biased in the free troposphere, this information on ozone features probably plays a non-negligible effect in the the tropospheric ozone budget, which will be studied in further studies. Studying the tropospheric ozone budget is out of the scope of this paper.

6 Conclusions

In this paper we show the benefit of high horizontal resolution and MLS ozone assimilation on STE events. We use assimilation of MLS ozone profiles to constrain the MOCAGE CTM in the UTLS at middle and high latitudes. The study is conducted over Europe at low horizontal resolution (2°) and high horizontal resolution (0.2°). The assimilation of MLS ozone tends to increase the ozone concentration in UTLS levels in polar and middle latitudes and we show the importance of such an increase on the free troposphere. It is shown that the assimilation increments, advected through the

ACPD
11, 33419–33463, 2011

tropopause, also affect significantly the free troposphere. The added value of MLS ozone assimilation and its impact on troposphere are illustrated using two case studies.

These case studies (23 June 2009 and 17 July 2009) which both show a stratospheric intrusion, are detailed in the paper. The combination of high horizontal resolution and MLS ozone assimilation allows an accurate estimate of UTLS ozone fields. High resolution runs are able to represent very thin filamentary structures of potential vorticity and ozone which characterise a STE. These structures of ozone are described more realistically in the MLS ozone analyses. The confidence of the ozone analyses is assessed by comparison against independent measurements from MOZAIC aircraft and WOUDC ozone sonde. In both cases, comparison with MOZAIC flight data show that the ozone analyses at the two resolutions provide a better description of the UTLS and the stratospheric intrusions, than the free model run. In particular, at high horizontal resolution the UTLS show fine ozone structures. In addition, the comparison with ozone sonde measurements shows that the high horizontal resolution improves the representation of the UTLS. The transport at high resolution in the free troposphere reveals a maximum of tropospheric ozone at 500 hPa (17 July 2009 case). However, we found a bias in the free troposphere between the ozone analysis and the in-situ data at the resolutions used. It is likely due to a too coarse model resolution in comparison to the MOZAIC data sampling. The model is unable to represent as strong gradients as shown in MOZAIC data. This affects significantly the UTLS by increasing the concentration of ozone transported into the free troposphere, and explains the bias.

Then, we calculate and discuss different estimates of the ozone fluxes through the tropopause using the free run, analyses and the high and low horizontal resolutions. We find that MLS ozone analyses tend to increase the ozone fluxes whereas the high horizontal resolution decreases it. Even though the ozone net flux estimates show significantly different results, the values estimated lie within the range found by other studies for similar conditions.

ACPD
11, 33419–33463, 2011

It has been shown that vertical structures in tropospheric ozone profiles appearing as laminae in high horizontal resolution MLS ozone analyses come from the UTLS at high latitudes. By using backward trajectories, we show that these structures which only appear at high resolution come from the UTLS region at high latitudes. In addition, we use MLS ozone analyses at high horizontal resolution to forecast the tropospheric ozone features. After 2.5 days the forecast vertical tropospheric profile is very close to the MLS ozone analysis which has a better representation of tropospheric ozone laminae structures than the free run. After 7 days the difference between forecast and MLS ozone analyses in the troposphere become significant (greater than 5 %). This confirms that improving the ozone in the UTLS region using MLS ozone data, improves the ozone distribution in the free troposphere revealing laminae structures in the ozone profile.

In order to improve the variability on tropospheric ozone but also to improve the absolute value of tropospheric ozone, we propose in a further study to extend the geometry of the observations assimilated by combining stratospheric limb observations with tropospheric column nadir observations.

Acknowledgements. This work was funded by the Centre National de Recherches Scientifiques (CNRS) and the Centre National de Recherches Météorologiques (CNRM) of Météo-France. VHP, JLA, LEA and WL are supported by the RTRA/STAE (POGEQA project). JLA thanks also the Région Midi Pyrénées (INFOAIR project). Thanks to the WOUDC to provide ozone sonde data sets. The authors acknowledge for the strong support of the European Commission, Airbus, and the Airlines (Lufthansa, Austrian, Air France) who carry free of charge the MOZAIC equipment and perform the maintenance since 1994. MOZAIC is presently funded by INSU-CNRS (France), Météo-France, and Forschungszentrum (FZJ, Julich, Germany). The MOZAIC data based is supported by ETHER (CNES and INSU-CNRS).

ACPD
11, 33419–33463, 2011

The publication of this article is financed by CNRS-INSU.

References

Ancellet, G., Pelon, J., Beekmann, M., Papayannis, A., and Mégie, G.: Ground based lidar studies of ozone exchanges between the stratosphere and the troposphere, J. Geophys. Res., 96, 22401–22421, 1991. 33437

Appenzeller, C. and Davies, H. C.: Structure of stratospheric intrusion into the troposphere, Nature, 358, 570–572, 1992. 33427

Appenzeller, C., Davies, H. C., and Norton, W. A.: Fragmentation of stratospheric intrusions, J. Geophys. Res., 101, 1435–1456, 1996. 33421, 33427, 33428

Bechtold, P., Bazile, E., Guichard, F., Mascart, P., and Richard, E.: A mass-flux convection scheme for regional and global models, Q. J. Roy. Meteor. Soc., 96, 869–886, 2001. 33423

Beekmann, M., Ancellet, G., and Mégie, G.: Climatology of tropospheric ozone in southern Europe and its relation to potential vorticity, J. Geophys. Res., 99, 841–853, 1994. 33421

Bencherif, H., Amraoui, L. E., Sernane, N., Massart, S., Charyulu, D. V., Hauchecorne, A., and Peuch, V.-H.: Examination of the 2002 major warming in the southern hemisphere using ground-based and Odin/SMR assimilated data: stratospheric ozone distributions and tropic/mid-latitude exchange, Can. J. Phys., 85, 1287–1300, 2007. 33425

Bousserez, N., Attié, J.-L., Peuch, V.-H., Michou, M., Pfister, G., Edwards, D., Emmons, L., Mari, C., Barret, B., Arnold, S. R., Heckel, A., Richter, A., Schlager, H., Lewis, A., Avery, M., Sachse, G., Browell, E. V., and Hair, J. W.: Evaluation of the MOCAGE chemistry transport model during the ICARTT/ITOP experiment, J. Geophys. Res., 112, D10S42, doi:10.1029/2006JD007595, 2007. 33423

Browning, K. A.: Evolution of a mesoscale upper tropospheric vorticity maximum and comma

ACPD

11, 33419–33463, 2011

cloud from a cloud-free two-dimensional potential vorticity anomaly, Q. J. Roy. Meteorol. Soc., 119, 883–906, doi:10.1002/qj.49711951302, 1993. 33428

Buis, S., Piacentini, A., and Déclat, D.: PALM: a computational framework for assembling high-performance computing applications, Concurrency Computat., Pract. Exper., 18, 231–245, doi:10.1002/cpe.914, 2006. 33424

Büker, M. L., Hitchmann, M. H., Tripoli, G. J., Pierce, R. B., Browell, E. V., and Avery, M. A.: Resolution dependence of cross-tropopause ozone transport over East Asia, J. Geophys. Res., 110, D03107, doi:10.1029/2004JD004739, 2005. 33421, 33437

Clark, H. L., Cathala, M.-L., Teyssèssdre, H., Cammas, J.-P., and Peuch, V.-H.: Cross-tropopause fluxes of ozone unsing assimilation of MOZAIC observations in a global CTM, Tellus, 59B, 39–49, 2007. 33421, 33434

Courtier, P., Freydier, C., Geleyn, J. F., Rabier, F., and Rochas, M.: The ARPEGE project at Météo France, in: Atmospheric Models, vol.2, 193–231, Workshop on Numerical Methods, Reading, UK, 1991. 33423

Crutzen, P. J., Lawrence, M. G., and Pöschl, U.: On the background photochemistry of tropospheric ozone, Tellus, 51A-B, 123–146, 1999. 33434

Dufour, A., Amodei, M., Ancellet, G., and Peuch, V.-H.: Observed and modelled "chemical weather" during ESCOMPTE, Atmos. Res., 74, 161–189, doi:10.1016/j.atmosres.2004.04.013, 2005. 33423

Ebel, A., Hass, H., Jakobs, H. J., Laube, M., Memmesheimer, M., Oberreuter, A., Geiss, H., and Kuo, Y. H.: Simulation of ozone intrusion caused by a tropopause fold and cut off low, Atmos.-Environ., 25, 2131–2144, 1991. 33421

El Amraoui, L., Peuch, V.-H., Ricaud, P., Massart, S., Semane, N., Teyssèdre, H., Cariolle, D., and Karcher, F.: Ozone loss in the 2002–2003 Arctic vortex deduced from the assimilation of Odin/SMR O3 and N2O measurements: N2O as a dynamical tracer, Q. J. Roy. Meteor. Soc., 134, 217–228, doi:10.1002/qj.191, 2008a. 33423, 33425

El Amraoui, L., Semane, N., Peuch, V.-H., and Santee, M. L.: Investigation of dynamical processes in the polar stratospheric vortex during the unusually cold winter 2004/2005, Geophys. Res. Lett., 35, L03803, doi:10.1029/2007GL031251, 2008b. 33425

El Amraoui, L., Attié, J.-L., Semane, N., Claeyman, M., Peuch, V.-H., Warner, J., Ricaud, P., Cammas, J.-P., Piacentini, A., Josse, B., Cariolle, D., Massart, S., and Bencherif, H.: Midlatitude stratosphere – troposphere exchange as diagnosed by MLS O_3 and MOPITT CO assimilated fields, Atmos. Chem. Phys., 10, 2175–2194, doi:10.5194/acp-10-2175-2010,

ACPD
11, 33419–33463, 2011

2010. 33422, 33425
Fisher, M. and Andersson, E.: Developments in 4D-Var and Kalman filtering, in: Technical Memorandum Research Department, vol. 347, ECMWF, Reading, UK, 2001. 33424
Froidevaux, L., Jiang, Y. B., Lambert, A., Livesey, N. J., Read, W. G., Waters, J. W., Browell, E. V., Hair, J. W., Avery, M. A., McGee, T. J., Twigg, L. W., Sumnicht, G. K., Jucks, K. W., Margitan, J. J., Sen, B., Stachnik, R. A., Toon, G. C., Bernath, P. F., Boone, C. D., Walker, K. A., Filipiak, M. J., Harwood, R. S., Fuller, R. A., Manney, G. L., Schwartz, M. J., Daffer, W. H., Drouin, B. J., Cofield, R. E., Cuddy, D. T., Jarnot, R. F., Knosp, B. W., Perun, V. S., Snyder, W. V., Stek, P. C., Thurstans, R. P., and Wagner, P. A.: Validation of Aura Microwave Limb Sounder stratospheric ozone measurements, J. Geophys. Res., 113, D15S20, doi:10.1029/2007JD008771, 2008. 33425
Geer, A. J., Lahoz, W. A., Bekki, S., Bormann, N., Errera, Q., Eskes, H. J., Fonteyn, D., Jackson, D. R., Juckes, M. N., Massart, S., Peuch, V.-H., Rharmili, S., and Segers, A.: The ASSET intercomparison of ozone analyses: method and first results, Atmos. Chem. Phys., 6, 5445–5474, doi:10.5194/acp-6-5445-2006, 2006. 33425
Gouget, H., Vaughan, G., Marenco, A., and Smit, H. G. J.: Decay of a cut-off low and contribution to stratosphere-troposphere exchange, J. Geophys. Res., 126, 1117–1141, doi:10.1002/qj.49712656414, 2000. 33428
Grewe, V. and Dameris, M.: Calculating the global mass exchange between stratosphere and troposphere, Ann. Geophys., 14, 431–442, doi:10.1007/s00585-996-0431-x, 1996. 33421, 33434
Hauchecorne, A., Godin, S., Marchand, M., Heese, B., and Souprayen, C.: Quantification of the transport of chemical constituents from the polar vortex to midlatitudes in the lower stratosphere using the high-resolution advection model MIMOSA and effective diffusivity, J. Geophys. Res., 107, 8289, doi:10.1029/2001JD000491, 2002. 33421
Hitchman, M. H., Büker, M. L., Tripoli, G. J., Browell, E. V., Grant, W. B., McGee, T. J., and Burris, J. F.: Nonorographic generation of Arctic polar stratospheric clouds during December 1999, J. Geophys. Res., 108, 8325, doi:10.1029/2001JD001034, 2003. 33437
Hoerling, M. P., Schaak, T. K., and Lenzen, A. J.: Global objective tropopause analysis, Mon. Weather Rev., 119, 1816–1831, 1991. 33435
Hollingsworth, A., Engelen, R., Textor, C., Boucher, O., Chevallier, F., Dethof, A., Elbern, H., Eskes, H., Flemming, J., Granier, C., Kaiser, J. W., Morcrette, J. J., Rayner, P., Peuch, V.-H., Rouïl, L., and the GEMS Consortium: Toward a monitoring and forecasting system for

ACPD
11, 33419–33463, 2011

atmospheric composition: The GEMS Project, B. Am. Meteorol. Soc., 89, 1147–1164, 2008. 33423
Holton, J. R., Haynes, P. H., McIntyre, M. E., Douglass, A. R., Rood, R. B., and Pfister, L.: Stratosphere-troposphere exchange, Rev. Geophys., 4, 403–439, 1995. 33421, 33433
IPCC 1996: IPCC, Climate Change 1995. The Science of Climate Change, edited by: Houghton, J. T., Meira Filho, L. G., Callander, B. A., Harris, N., Kattenberg, A., and Maskell, K., 1996. 33421
Jing, P., Cunnold, D. M. , Wang, H. J., and Yang, E. S.: Isentropic Cross-Tropopause Ozone Transport in the Northern Hemisphere, J. Atmos. Sci., 61, 1068–1078, 2004. 33421, 33434
Josse, B., Simon, P., and Peuch, V.-H.: Radon global simulation with the multiscale chemistry transport model MOCAGE, Tellus, 56, 339–356, 2004. 33423
Kalnay, E.: Atmospheric modeling, data assimilation, and predictability., University Press, Cambridge, 2003. 33422
Lahoz, W. A., Errera, Q., Swinbank, R., and Fonteyn, D.: Data assimilation of stratospheric constituents: a review, Atmos. Chem. Phys., 7, 5745–5773, doi:10.5194/acp-7-5745-2007, 2007. 33424
Lamarque, J. F. and Hess, P. G.: Cross-Tropopause mass-exchange and potential vorticity budget in a simulated tropopause folding, J. Atmos. Sci., 51, 2246–2269, 1994. 33437
Law, K. S., Plantevin, P.-H., Thouret, V., Marenco, A., Asman, W. A. H., Lawrence, M., Crutzen, P. J., Muller, J.-F., Hauglustaine, D. A., and Kanakidou, M.: Comparison between global chemistry transport model results and Measurement of Ozone and Water Vapor by Airbus In-Service Aircraft (MOZAIC) data, J. Geophys. Res., 105, 1503–1525, doi:10.1029/1999JD900474, 2000. 33422
Leblanc, T., Tripathi, O. P., McDermid, I. S., Froidevaux, L., Livesey, N. J., Read, W. G., and Waters, J. W.: Simultaneous lidar and EOS MLS measurements, and modeling, of a rare polar ozone filament event over Mauna Loa Observatory, Hawaii, Geophys. Res. Lett., 33, L16801, doi:10.1029/2006GL026257, 2006. 33422
Lefèvre, F., Brasseur, G. P., Folkins, I., Smith, A. K., and Simon, P.: Chemistry of the 1991–1992 stratospheric winter: three dimensional model simulations, J. Geophys. Res., 99, 8183–8195, 1994. 33423
Louis, J.-F.: Parametric model of vertical eddy fluxes in the atmosphere, Bound. Lay. Meteorol., 17, 187–202, 1979. 33423
Luk'yanov, A. N., Karpechko, A. Y., Yushkov, V. A., Korshunov, L. I., Khaikin, S. M., Gan'shin,

ACPD
11, 33419–33463, 2011

A. V., Kyro, E., Kivi, R., Maturilli, M., and Voemel, H.: Estimation of water-vapor and ozone transport in the upper troposphere-lower stratosphere and fluxes through the tropopause during the field campaign at the Sodankyla station (Finland), Izvestiya Atmospheric and Oceanic Physics, 45, 294–301, doi:10.1134/S0001433809030037, 2009. 33421, 33437

Marchand, M., Godin, S., Hauchecorne, A., Lefèvre, F., Bekki, S., and Chipperfield, M.: Influence of polar ozone loss on northern midlatitude regions estimated by a high-resolution chemistry transport model during winter 1999/2000, J. Geophys. Res., 108, 8326, doi:10.1029/2001JD000906, 2003. 33421

Marenco, A., Thouret, V., Nedelec, P., Smit, H. G., Helten, M., Kley, D., Karcher, F., Simon, P., Law, K., Pyle, J., Poschmann, G., Wrede, R. V., Hume, C., and Cook, T.: Measurement of ozone and water vapour by Airbus in-service aircraft: the MOZAIC airborne program, an overview, J. Geophys. Res., 103, 25631–25242, 1998. 33431

Massart, S., Piacentini, A., Cariolle, D., El Amraoui, L., and Semane, N.: Assessment of the quality of the ozone measurements from the Odin/SMR instrument using data assimilation, Can. J. Phys., 85, 1209–1223, 2007. 33425

Murphy, D. M. and Fahey, D. W.: An estimate of the flux of stratospheric reactive nitrogen and ozone into the troposphere., J. Geophys. Res., 99, 5325–5332, 1994. 33434

Olsen, M. A., Douglass, A. R., and Schoeberl, M. R.: stimating downward cross-tropopause ozone flux using column ozone and potential vorticity., J. Geophys. Res., 107, 4636, doi:10.1029/2001JD002041, 2002. 33421, 33434

Olsen, M. A., Douglass, A. R., and Schoeberl, M. R.: A comparison of Northern and Southern Hemisphere cross-tropopause ozone flux, Geophys. Res. Lett. , 30, 1412, doi:10.1029/2002GL016538, 2003. 33421, 33434

Peuch, V.-H., Amodei, M., Barthet, T., Cathala, M.-L., Michou, M., and Simon, P.: MOCAGE, MOdéle de Chimie Atmosphérique à Grande Echelle, in: Proceedings of Météo France: Workshop on atmospheric modelling, 33–36, Toulouse, France, 1999. 33422, 33423

Postel, G. A. and Hitchman, H. M.: A climatology of Rossby wave breaking along the subtropical tropopause, J. Atmos. Sci., 56, 359–373, 1999. 33427

Ramaswamy, V., Boucher, O., Haigh, J., Hauglustaine, D., Haywood, J., Myhre, G., Nakajima, T., Shi, G. Y., and Solomon, S.: Radiative Forcing of Climate Change, in: Climate Change 2001: The Scientific Basis. Contribution of working group I to the Third Assessment Report of the Intergovernmental Panel on Climate Change, Cambridge Univ. Press, New York, 349–416, 2001. 33420

ACPD
11, 33419–33463, 2011

Rouïl, L., Honoré, C., Vautard, R., Beekmann, M., Bessagnet, B., Malherbe, L., Meleux, F., Dufour, A., Elichegaray, C., Flaud, J.-M., Menut, L., Martin, D., Peuch, A., Peuch, V.-H., and Poisson, N.: An Operational Forecasting and Mapping System for Air Quality in Europe, B. Am. Meteor. Soc., 90, 73–83, 2008. 33423

Semane, N., Peuch, V.-H., Amraoui, L. E., Bencherif, H., Massart, S., Cariolle, D., Attié, J.-L., and Abidab, R.: An observed and analysed stratospheric ozone intrusion over the high Canadian Arctic UTLS region during the summer of 2003, Q. J. Roy. Meteor. Soc., 133, 171–178, doi:10.1002/qj.141, 2007. 33422, 33425

Stockwell, W. R., Kirchner, F., Khun, M., and Seefeld, S.: A new mechanism for regional atmospheric chemistry modelling, J. Geophys. Res., 102, 25847–25879, 1997. 33423

Stohl, A., Wernli, H., James, P., Bourqui, M., Forster, C., Liniger, M. A., Seibert, P., and Sprenger, M.: A new perspective of stratosphere-troposphere exchange, B. Am. Meteorol. Soc., 84, 1565–1573, doi:10.1175/BAMS-84-11-1565, 2003. 33421, 33433

Thorncroft, C. D., Hoskins, B. J., and McIntyre, M. E.: Two paradigms of baroclinic-wave life-cycle behaviour, Q. J. Roy. Meteorol. Soc., 119, 17–55, doi:10.1002/qj.49711950903, 1993. 33428

Thouret, V., Marenco, A., Logan, J., Nédélec, P., and Grouhel, C.: Comparisons of ozone measurements from the MOZAIC airborne program and the ozone sounding network at eight locations, J. Geophys. Res., 103, 25695–25720, 1998. 33431

Tripathi, O. P., Leblanc, T., McDermid, I. S., Lefèvre, F., Marchand, M., and Hauchecorne, A.: Forecast, measurement, and modeling of an unprecedented polar ozone filament event over Mauna Loa Observatory, Hawaii, J. Geophys. Res., 111, D20308, doi:10.1029/2006JD007177, 2006. 33421

Wargan, K., Pawson, S., Stajner, I., and Thouret, V.: Spatial structure of assimilated ozone in the upper troposphere and lower stratosphere, J. Geophys. Res., 115, D24316, doi:10.1029/2010JD013941, 2010. 33422

Waters, J. W., Froidevaux, L., Harwood, R. S., Jarnot, R. F., Pickett, H. M., Read, W. G., Siegel, P. H., Cofield, R. E., Filipiak, M. J., Flower, D. A., Holden, J. R., Lau, G. K. K., Livesey, N. J., Manney, G. L., Pumphrey, H. C., Santee, M. L., Wu, D. L., Cuddy, D. T., Lay, R. R., Loo, M. S., Perun, V. S., Schwartz, M. J., Stek, P. C., Thurstans, R. P., Boyles, M. A., Chandra, K. M., Chavez, M. C., Chen, G. S., Chudasama, B. V., Dodge, R., Fuller, R. A., Girard, M. A., Jiang, J. H., Jiang, Y. B., Knosp, B. W., LaBelle, R. C., Lam, J. C., Lee, K. A., Miller, D., Oswald, J. E., Patel, N. C., Pukala, D. M., Quintero, O., Scaff, D. M., Snyder, W. V., Tope, M. C., Wagner,

ACPD
11, 33419–33463, 2011

P. A., and Walch, M. J.: The Earth Observing System Microwave Limb Sounder (EOS MLS) on the Aura satellite, IEEE T. Geosci. Remote Sens., 44, 1075–7092, 2006. 33425

Wei, M. Y.: A new formulation of the exchange of mass and trace constituents between the stratosphere and troposphere, J. Atmos. Sci., 44, 3079–3086, 1987. 33421, 33434, 33437

World Meteorological Organization: Atmospheric Ozone: 1985, Global ozone research and monitoring project report no. 16, 1986. 33435

ACPD

11, 33419–33463, 2011

Table 1. Differences between average fluxes in absolute values calculated in the range of 2.5 PVU and 1.5 PVU. LR_a: Low Resolution Analysis, HR_a: High Resolution Analysis, LR_f: Low Resolution Free-run, HR_f: High Resolution Free-run. LR refers to 2° whereas HR refers to 0.2°.

	Case 1	Case 2
$(LR_a\text{-}LR_f)/LR_f$	86 %	109 %
$(HR_a\text{-}HR_f)/HR_f$	30 %	56 %
$(HR_f\text{-}LR_f)/LR_f$	−63 %	−68 %
$(HR_a\text{-}LR_a)/LR_a$	−74 %	−76 %
Domain Size	1×10^6 km^2	1.6×10^6 km^2
Duration	4.5 days	3.5 days

ACPD
11, 33419–33463, 2011

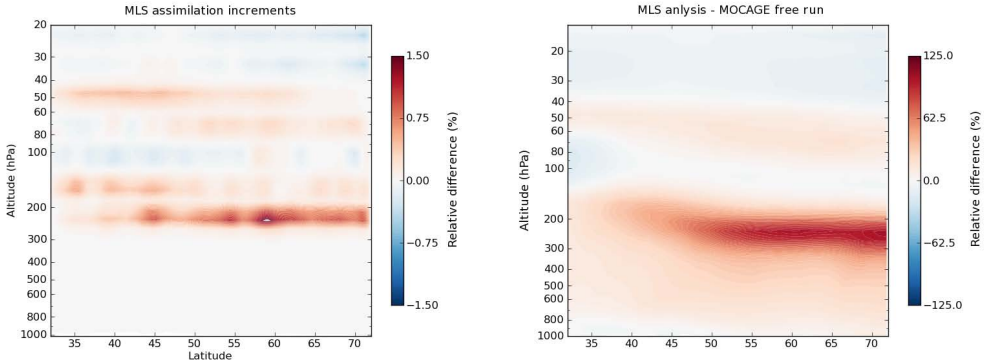

Fig. 1. Zonal means for the month of July 2009 over Europe: left hand side: increments of MLS ozone analyses at high horizontal resolution (0.2°) in relative difference in %; right hand side: MLS ozone analysis minus the associated equivalent MOCAGE free run at high horizontal resolution (0.2°) in relative difference in %.

ACPD
11, 33419–33463, 2011

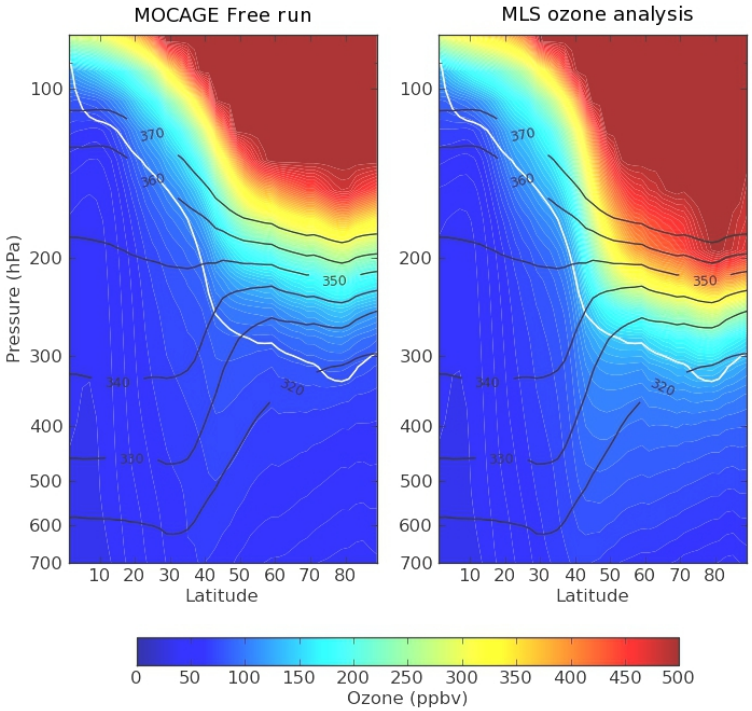

Fig. 2. Zonal means of ozone for the month of July 2009 in Northern Hemisphere (low resolution runs 2°). Left hand side: MOCAGE free run, right hand side: MLS ozone analysis. Black lines are the potential temperature, the white line represents the 2 PVU (an estimate of the tropopause height).

ACPD
11, 33419–33463, 2011

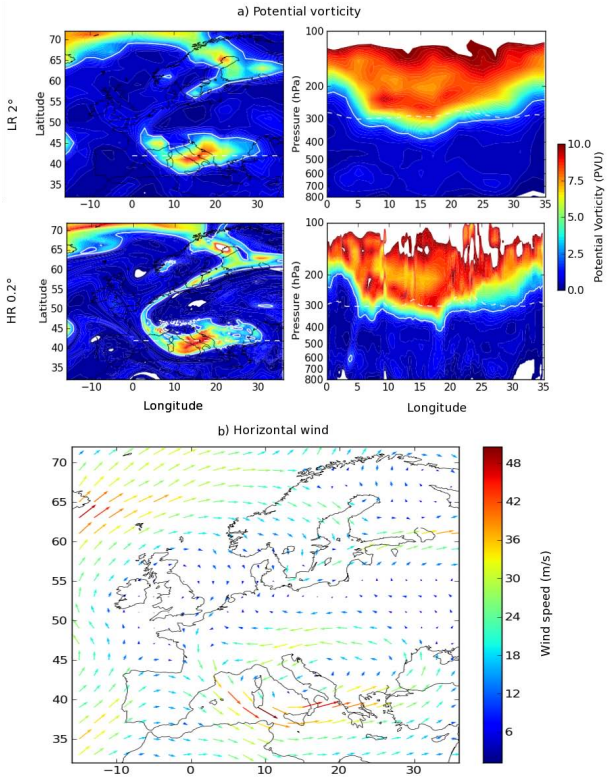

Fig. 3. Situation on 23 June 2009, 12:00 UT from ARPEGE analysis. **(a)** Potential vorticity fields, in potential vorticity unit (1 PVU = 1×10^6 K kg^{-1} m^2 s^{-1}) from low (2°) horizontal resolution simulation (top) and high horizontal resolution (0.2°) simulation (bottom). Left hand side panels show longitude-latitude fields; right hand side panels show longitude-pressure cross-sections. The white dashed line associates the vertical and the horizontal distribution by showing the same location between left hand side and right hand side panels. The white solid lines identify the 2 PVU contour. **(b)** Horizontal wind fields at LR near 300 hPa.

ACPD
11, 33419–33463, 2011

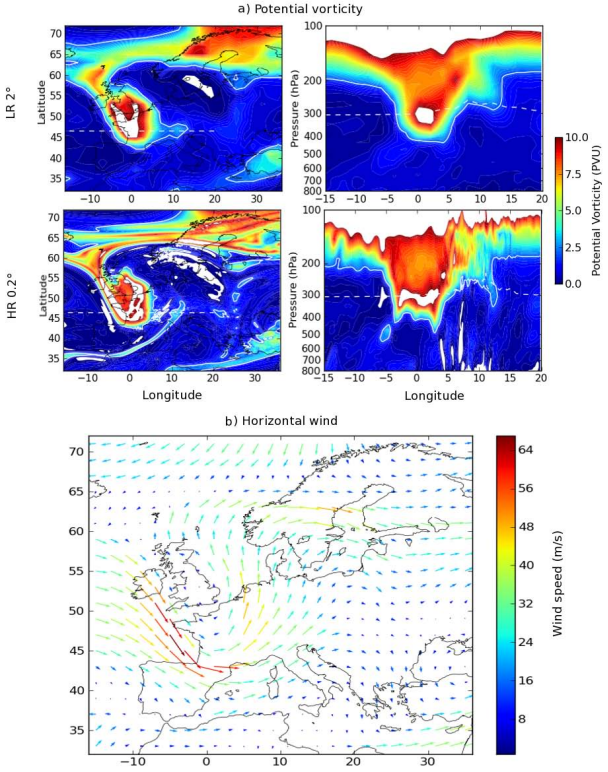

Fig. 4. Situation on 17 July 2009, 15:00 UT from ARPEGE analysis. **(a)** Potential vorticity fields, in potential vorticity unit (1 PVU = 1×10^6 K kg^{-1} m^2 s^{-1}) from low horizontal resolution (2°) simulation (top) and high horizontal resolution (0.2°) simulation (bottom). Left hand side panels show longitude-latitude fields; right hand side panels show longitude-pressure cross-sections. The white dashed line associates the vertical and the horizontal distribution by showing the same location between left hand side and right hand side panels. The white solid lines identify the 2 PVU contour. **(b)** Horizontal wind fields at LR near 300 hPa.

ACPD
11, 33419–33463, 2011

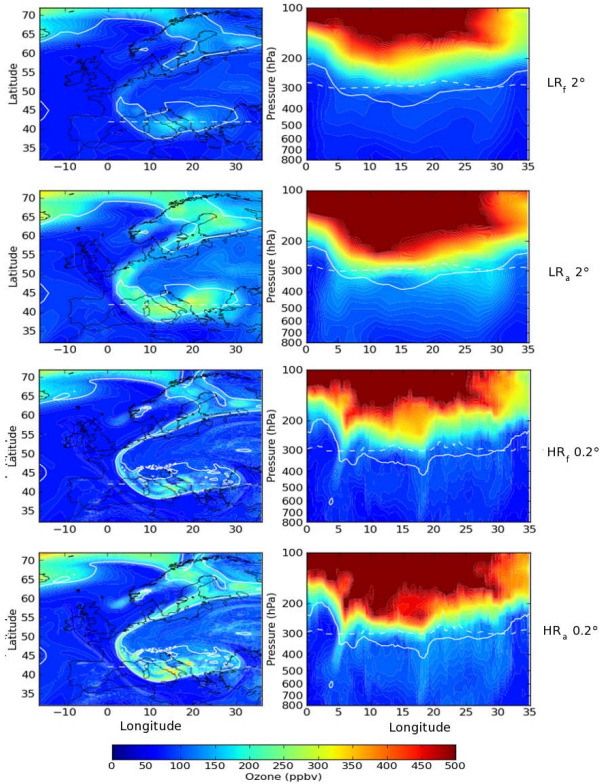

Fig. 5. Ozone fields for 23 June 2009, 12:00 UT, in ppbv (parts per billion by volume) for various experiments: LR_f: Low Resolution (2°) free run; LR_a: Low Resolution (2°) analyses; HR_f: High Resolution (0.2°) free run and HR_a: High Resolution (0.2°) analyses. Left hand side panels show longitude-latitude fields; right hand side panels show longitude-pressure cross-sections. White dashed line associate vertical and horizontal distribution by showing the same location between left hand side and right hand side panels. The white solid lines identify the 2 PVU contour.

ACPD
11, 33419–33463, 2011

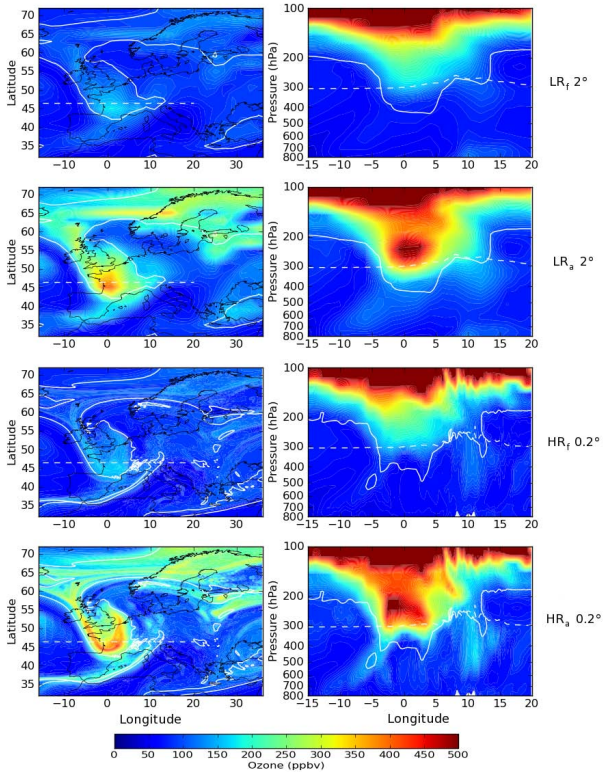

Fig. 6. Ozone fields for 17 July 2009, 15:00 UT, in ppbv (parts per billion by volume) for various experiments: LR_f: Low Resolution (2°) free run; LR_a: Low Resolution (2°) analyses; HR_f: High Resolution (0.2°) free run and HR_a: High Resolution (0.2°) analyses. Left hand side panels show longitude-latitude fields; right hand side panels show longitude-pressure cross-sections. White dashed line associate vertical and horizontal distribution by showing the same location between left hand side and right hand side panels. The white solid lines identify the 2 PVU contour.

ACPD
11, 33419–33463, 2011

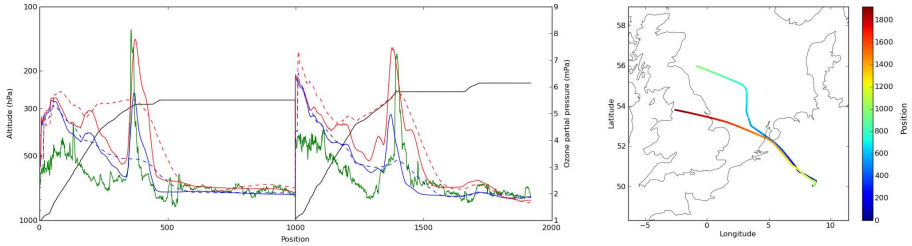

Fig. 7. Left hand side panel: ozone data from MOZAIC (green line), free MOCAGE run (blue lines) and analyses fields (red lines), in mPa (10^{-3} Pascals, right y-axis); flight level (black line), in hPa (10^{2} Pascals, left y-axis). Low resolution (2°) and high resolution (0.2°) results are marked as dashed lines and solid lines, respectively. Right hand side panel: flight tracks on 23 June 2009. Position 0 to 1000: starting at Frankfurt (50° N, 8° E, Germany, 08:13 UT) to Calgary (51° N, 114° W, Canada). Position 1000 to 1900: starting at Frankfurt (50° N, 8° E, Germany, 13:00 UT) to Philadelphia (39° N, 75° W, US).

ACPD
11, 33419–33463, 2011

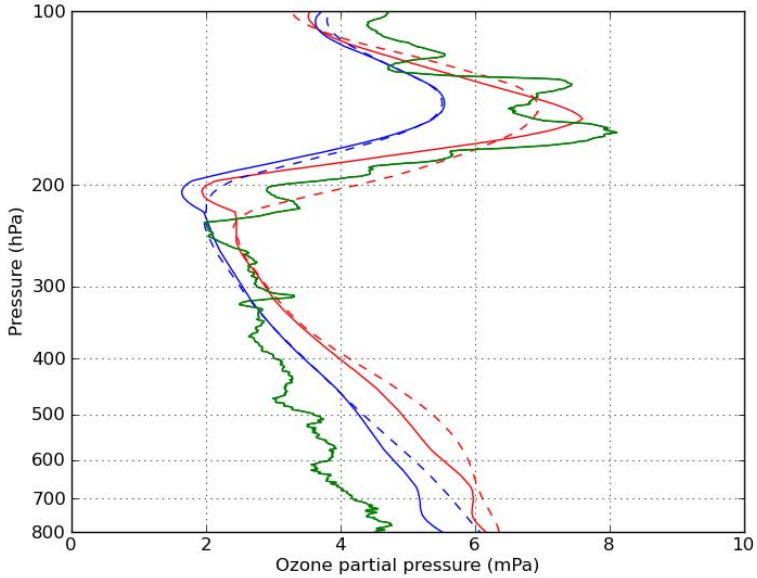

Fig. 8. Ozone profiles in mPa from a sonde over Legionowo (52.4° N, 21.97° E, Poland; green line, launched at 11:17 UT on 24 June 2009), from the free MOCAGE run (blue lines) and from analyses (red lines). Low resolution (2°) and high resolution (0.2°) results are represented by dashed and solid lines, respectively.

ACPD
11, 33419–33463, 2011

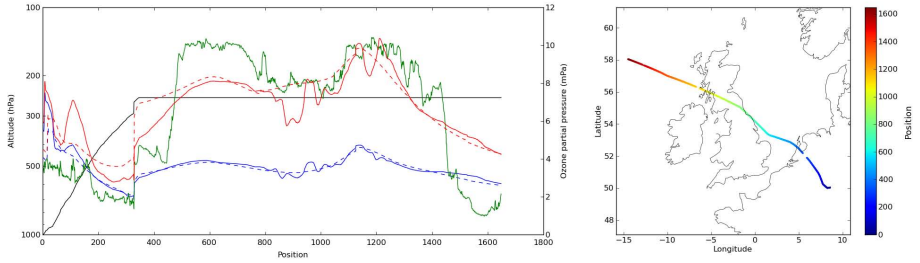

Fig. 9. Left hand side panel: ozone data from MOZAIC (green line), free MOCAGE run (blue lines) and analyses fields (red lines), units of mPa (right y-axis); flight level (black line), units of hPa (left y-axis). Low resolution (2°) and righ resolution (0.2°) results are marked as dashed lines and solid lines, respectively. Right hand side panel: flight track on 17 july 2009. Position 0 to 1700: starting at Frankfurt (50° N, 8° E, Germany, 11:57 UT) to Atlanta (33° N, 84°, US).

ACPD
11, 33419–33463, 2011

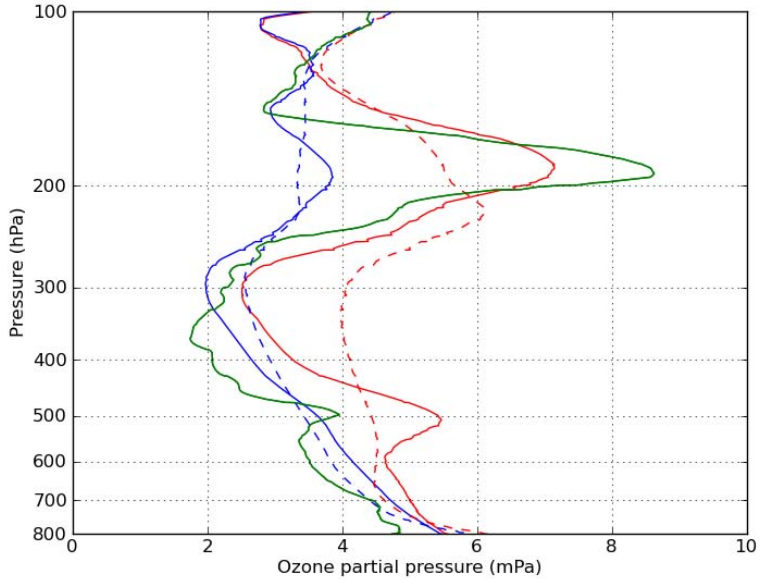

Fig. 10. Ozone profiles, mPa, from a sonde over Payerne (46.5° N, 6.6° E; green line, launched at 11:00 UT on 17 July 2009), from the free MOCAGE run (blue lines) and from analyses (red lines). Low resolution (2°) and high resolution (0.2°) results are represented by dashed and solid lines, respectively.

ACPD
11, 33419–33463, 2011

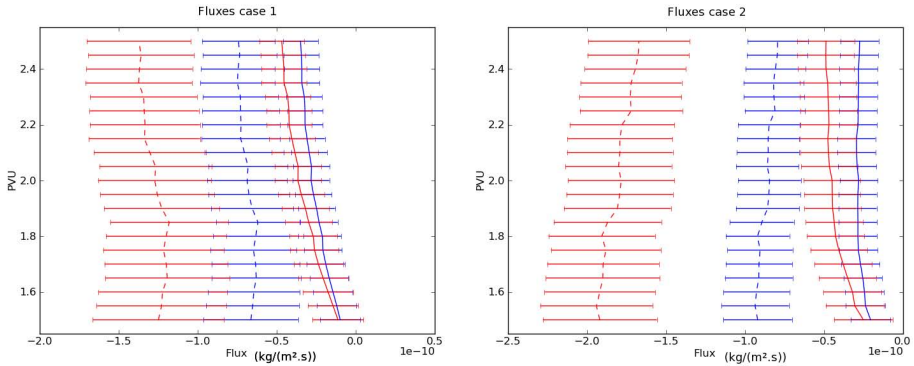

Fig. 11. Sensivity flux ($kg\,m^{-2}\,s^{-1}$) from free MOCAGE run (blue lines) and from analyses (red lines). Low resolution (2°) and high resolution (0.2°) results are represented by dashed and solid lines, respectively following different PV value in a range between 1.5 PVU and 2.5 PVU. Left case study 1: fluxes are estimated from 20 June, 06:00 UT, to 24 June, 18:00 UT. Right case study 2: fluxes are estimated from 16 July, 06:00 UT, to 19 July, 18:00 UT.

ACPD
11, 33419–33463, 2011

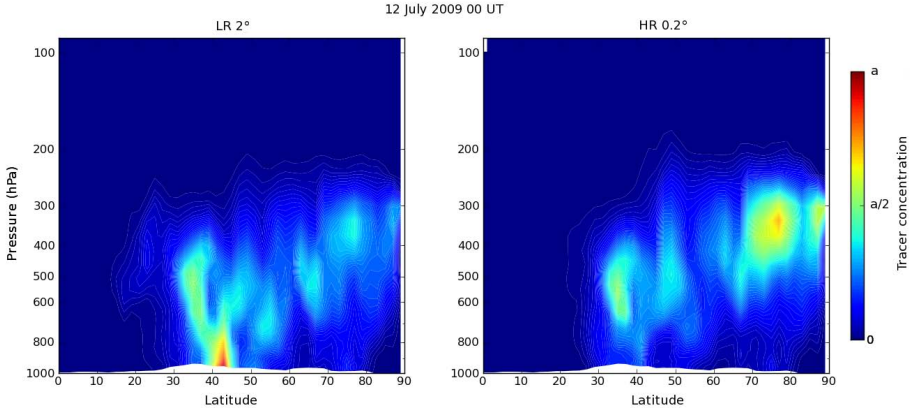

Fig. 12. Zonal means of a tracer initialised backward trajectories. Left hand side: Low Resolution (LR 2°), right hand side: High Resolution (HR 0.2°). Tracer concentration values are arbitrary: from 0 to a (the maximum value).

ACPD
11, 33419–33463, 2011

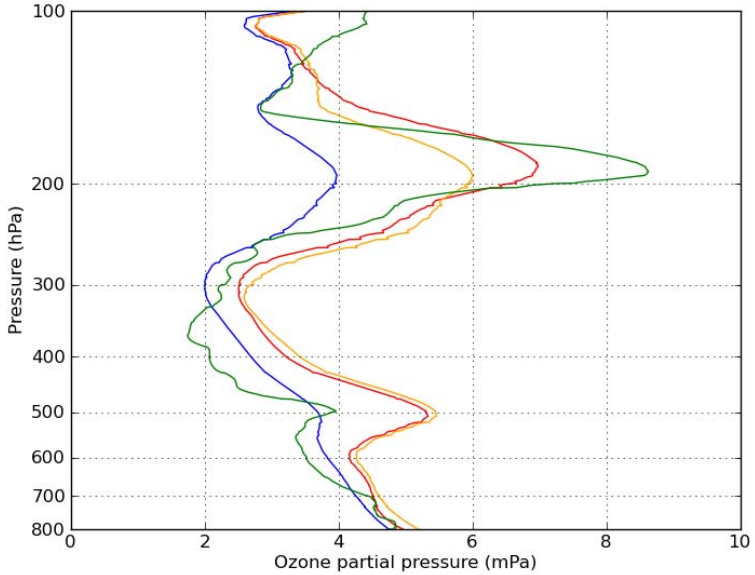

Fig. 13. Ozone profiles, mPa, from a sonde over Payerne (46.5° N, 6.6° E; green line, launched at 11:00 UT on 17 July 2009), from the free MOCAGE run (blue line), from analyses (red line) and forecasted run initialised with MLS anlyses at 00:00 UT on 15 July 2009 (orange line). All experiments are from High Resolution (0.2°) runs.

ACPD
11, 33419–33463, 2011

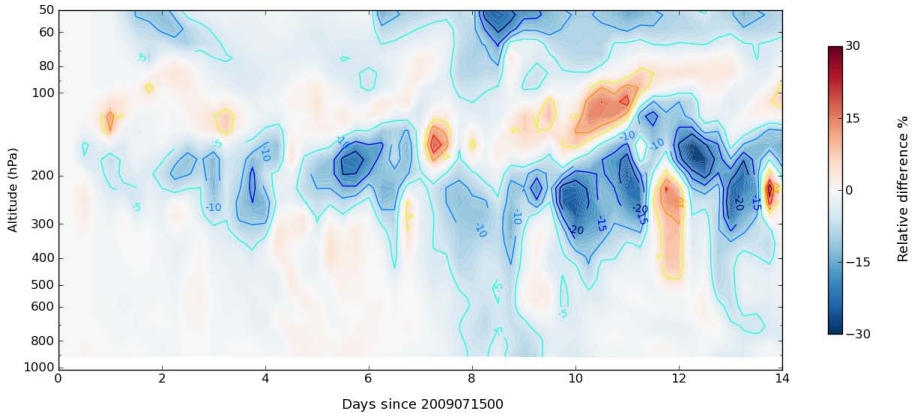

Fig. 14. Hovmuller diagram of the mean profile: (Forecast-MLS ozone analyses) in %, between 44° N–48° N and 5° W–9° W (Switzerland). Forecast is initialised from MLS ozone analyses on 15 July 2009 00:00 UT.

ACPD
11, 33419–33463, 2011